JOURNAL OF SOLID STATE CHEMISTRY 4, 430–446 (1972)

CS Families Derived From the ReO_3 Structure Type: An Electron Microscope Study of Reduced WO_3 and Related Pseudobinary Systems

L. A. BURSILL AND B. G. HYDE

School of Chemistry, University of Western Australia, Nedlands, Western Australia 6009

Received August 12, 1971

A broad survey of some ReO_3-related CS structures has been carried out by means of an electron microscopy/diffraction study of the systems WO_x and $(W^{6+},M^{5+})O_x$ with M = V, Nb, Ta and $2.90 \leqslant x < 3.00$; MoO_x and $(W,Mo)O_x$; $Nb(O,F)_x$ with $2.75 \leqslant x \leqslant 2.96$; as well as V_2MoO_8. The observations give a broader view of the field than was previously possible. (i) They reveal the expected "swinging" of the CS planes when the compositions and/or the component ions are varied. (ii) They provide information on the degree of long-range order and the types of defect present. (iii) They throw further light on the likely mechanism by which the composition changes when a CS structure is reduced or oxidized. These topics are discussed, and an attempt is made to systematize all the observations into a coherent picture incorporating previously available information. This necessitates changing some earlier, dubious conclusions from X-ray diffraction studies.

1. Introduction

The ordered, ReO_3-related, one-dimensional crystallographic shear (CS) structures that have been reported are listed in Table I. Three CS planes have been recognized, (102), (103) and (001), all with the displacement vector $\frac{1}{2}[10\bar{1}]$.[1] With the exception of $W_{50}O_{148}$ the structures are in excellent agreement with those determined or predicted by Magnéli (*1*). According to the structure reported for $W_{50}O_{148}$ (*2*) this is better denoted as $W_{25}O_{73+1}$: a (103) CS-type $W_{25}O_{73}$, with an interstitial oxygen added to give agreement between the measured composition and that derived from the structure analysis. The *c* axis is twice the ideal *c*, and so the formula becomes $2.W_{25}O_{73+1} = W_{50}O_{148}$.

Limited electron-microscopic studies have provided a little more information. Tilley (*3*) observed {102} CS planes in very slightly reduced tungsten trioxide. Allpress and Gadó (*4*) observed poorly ordered (103) CS phases W_nO_{3n-2} with $12 \lesssim n \lesssim 28$ in a sample of mean composition $WO_{2.90}$. Spyridelis, Delavignette and Amelinckx (*5*) observed faults in "nonstoichiometric" $WO_{3-\delta}$, later interpreted (*6*) as (001) CS planes very widely spaced (16 nm). We have observed the formation of random {001} CS planes in slightly reduced NbO_2F (*7*).

Implicit in Magnéli's homologous series, and explicitly suggested by Anderson and Hyde (*8*, *9*), is the possibility of other CS planes (*h*0*l*), with the

TABLE I

REPORTED ReO_3-RELATED (ONE-DIMENSIONAL) CS STRUCTURES

Compound	Formula	*n*	CS plane	Reference
$(Mo,W)O_x$	M_nX_{3n-1}	8, 9, 10, 11, 12	102	(*1*)
		14, > 14		(*16*)
$W_{20}O_{58}$	M_nX_{3n-2}	20	103	(*11*)
WO_x	M_nX_{3n-2}	12 to 28	103	(*4*)
$W_{35}Ta_4O_{115}$	M_nX_{3n-2}	39	103	(*13*)
$W_{40}O_{118}$	M_nX_{3n-2}	40	103	(*22*)
$W_{50}O_{148}$[a]	M_nX_{3n-2}	50	103	(*2*)
$(W,Nb)O_x$	M_nX_{3n-1}?	~13, ~17	?	(*12*)
V_2O_5	M_nX_{3n-1}	2	001	(*23*)
R-Nb_2O_5	M_nX_{3n-1}	2	001	(*24*)
$Mo_{0.6}V_{1.4}O_5$	M_nX_{3n-1}	2	001	(*25*)
$W_{0.75}V_{1.25}O_5$	M_nX_{3n-1}	2	001	(*15*)
Nb_3O_7F	M_nX_{3n-1}	3	001	(*26*)
V_2MoO_8	M_nX_{3n-1}	3	001	(*27*)

[a] But see text, p. 430.

[1] Unless otherwise indicated, indices refer to an ReO_3 unit cell or subcell.

same displacement vector $\frac{1}{2}[10\bar{1}]$. Some of these possibilities were also suggested by Magnéli (*1*). Analogous possibilities for *rutile*-derived CS structures have recently been observed (*10*): in this case the CS planes rotate between $(121)_r$ and $(132)_r$,[2] the general indices being

$$(hkl)_r = p(121)_r + q(011)_r.$$

Studies of the ternary system $(Mo_{1-a}, W_a)O_{2.90}$ by Magnéli et al. (*11*) indicated that, as a increased, (102) CS homologues M_nO_{3n-1} of increasing n occurred; i.e., the deduced values of $x = O/M$ increased although the prepared compositions were constant at $x = 2.90$. In view of the "rutile" results (*10*) and the obvious difficulty of determining accurate CS plane indices from X-ray diffraction patterns (*10*, *11*) it seemed to us more likely that, as a increased, the CS planes rotated from (102) in $Mo_{10}O_{29}$ ($n = 10$ in M_nO_{3n-1}) towards (103) which obtains in $W_{20}O_{58}$ ($n = 20$ in M_nO_{3n-2}) *at constant composition* $MO_{2.90}$. This alternative hypothesis was found to be quite consistent with the measured c axes, i.e., CS interplanar spacings D_{sp}.

These considerations, our doubts about the "$W_{50}O_{148}$" structure (*2*), the apparent inconsistency between the observations of Tilley (*3*) and Amelinckx et al. (*5*, *6*) on slightly reduced WO_3 [(102) and (001) CS planes, respectively], and the obvious gap between $WO_{3-\delta}$ and the (103) CS phase $W_{20}O_{58}$ ($WO_{2.90}$) [by no means closed by the exploratory X-ray diffraction studies of Roth and Waring (*12*) and Gadó and Magnéli (*13*)] all provided cogent reasons for a more comprehensive electron diffraction/microscopy study of ReO_3-related CS structures $(A^{6+}_{1-2b}, B^{5+}_{2b})O_{3-b}$. In addition to binary systems (with A = B) we have also investigated the effect of substituting various group V cations in WO_3, i.e., the pseudobinary systems $B_2O_5 + WO_3$.

2. Structural Considerations

Any ReO_3-type plane may be resolved into two components

$$(h0l) = p(001) + q(101)$$
$$= (q, 0, p + q).$$

Figure 1 shows that in an $(h0l)$ CS plane the (001) component is responsible for the composition change, giving families $M_nO_{3n-p} = M_nO_{3n-l+h}$, and the (101) component is a stoichiometric antiphase boundary (APB). [For terminology see Ref. (*14*)]. For (102) CS $p = 1$ and $q = 1$; for (103) $p = 2$ and $q = 1$; and for (001) $p = \infty$ and $q = 1$.

[2] The subscript r denotes indices based on the rutile cell or subcell.

The number of edge-shared pairs of $[MO_6]$ octahedra in unit length of CS plane is $(p + q)$ [= Magnéli's m (*1*)]; and they are arranged in q separate groups, in each of which the edge-shared pairs are joined by further edge sharing to produce a zig-zag strip. The simplest situation is for $q = 1$ when all groups are identical and each contains $(p + 1)$ edge-shared pairs. Then

$$(h0l) = p(001) + (101)$$
$$= (1, 0, p + 1).$$

In this case, as p increases, the CS plane changes discontinuously from (102) to (103), (104), ..., and eventually to $(10\infty) = (001)$ (a total angular range of $26\frac{1}{2}° = 0.46$ rad). If $q \geqslant 1$ an unlimited number of intermediate CS planes is possible; e.g., if $p = 3$, $q = 2$ the CS plane is parallel to (205), and along it groups of four and six edge-shared octahedra alternate. In a very real sense these intermediate CS planes $(h0l)$ are ordered intergrowths of the end members (101) and (001); and the intermediate CS structures are ordered intergrowths of columns of the primary structures $M_{n'}O_{3n'}$ and M_nO_{3n-1}. The (001) segments of the CS planes are strips of M_2O_5 structure (V_2O_5, R-Nb_2O_5), and therefore provide the correct number of cation sites to accommodate the 5-valent cations in $MO_{3-\delta}$. The ideal unit cells are identical, whether the pentavalent cations are ordered on to these sites or whether they are randomly distributed over all cation sites.

3. Preparation and Examination of Specimens

The starting materials were the following powders: Mo, BDH; W, Koch-Light 4*N*; MoO_3, Koch-Light 3*N*; WO_3, Koch-Light 3*N*; V_2O_5, Koch-Light 2*N*; Ta_2O_5, Koch-Light 3*N*; Nb_2O_5, Koch-Light < 3*N*; NbO_2F, prepared by dissolving Nb_2O_5 in 48% HF in a platinum crucible, and evaporating to dryness.

Appropriate weighed mixtures were sealed, in air or vacuum as required, in quartz glass or platinum tubes. They were then subjected to the various heat treatments listed in Table II.

The products were fractured between glass slides or in an agate pestle and mortar, and then mounted on specimen grids and examined in a JEM 6A or Elmiskop 101 electron microscope equipped with a goniometer stage and anticontamination device.

4. Identification of CS Plane $(h0l)$, and n in M_nO_{3n-p}

All planes $(h0l)$ lie in the zone [010], which must therefore be attained for positive identification of $(h0l)$. Since the displacement vector has a collapse

component of approx $\frac{1}{2}|l-h|=\frac{1}{2}p$, the CS plane spacing is

$$D_{sp} \doteq d_{h0l}(n-\tfrac{1}{2}p),$$

and there will be $(n-\frac{1}{2}p)$ "superlattice" spots along g($h0l$).

5. Observations

5.1. $MoO_{2.90}$

Two separate phases could be distinguished optically. By electron diffraction they were identified as unreduced MoO_3, and Mo_9O_{26} with well-ordered

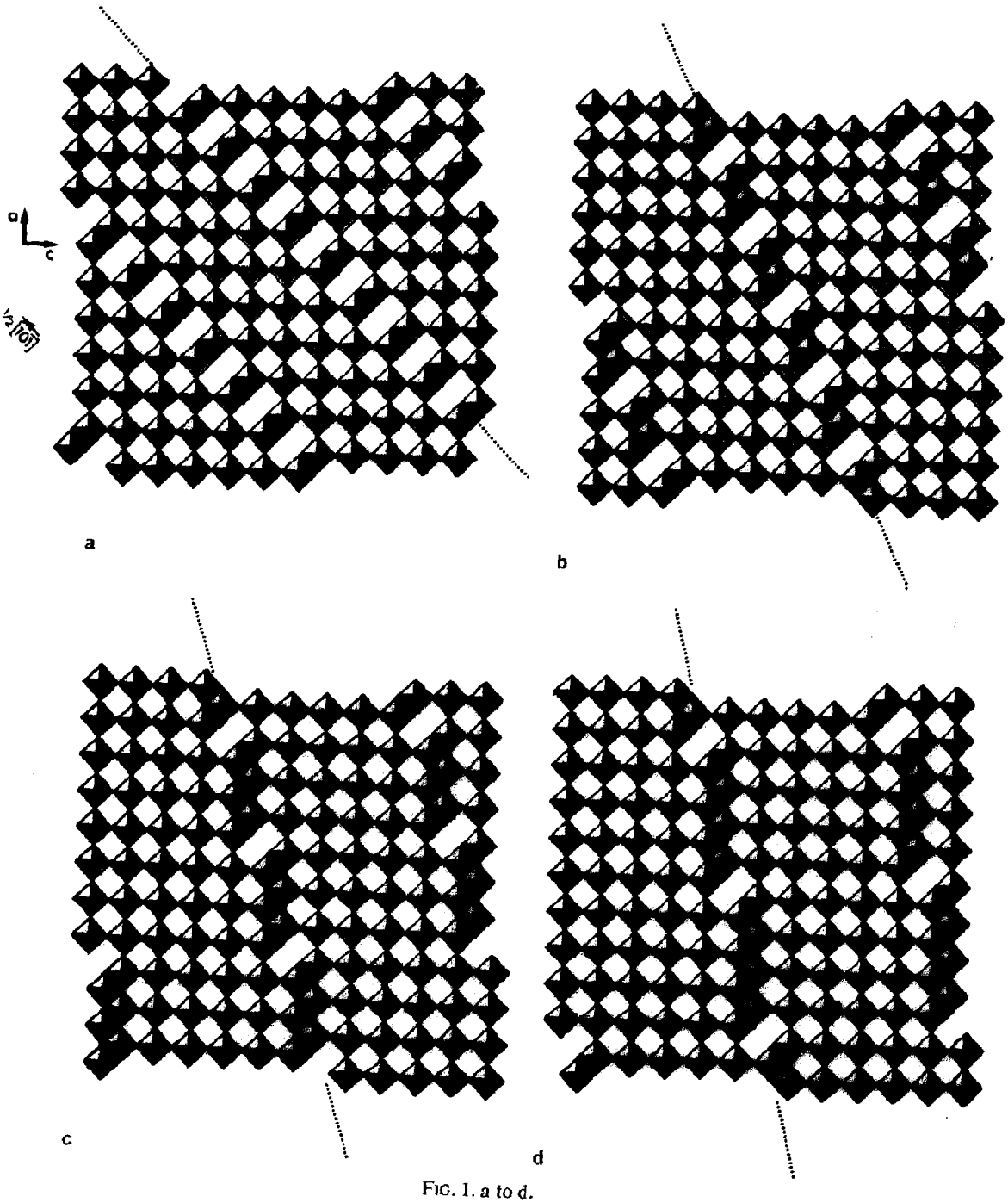

FIG. 1. a to d.

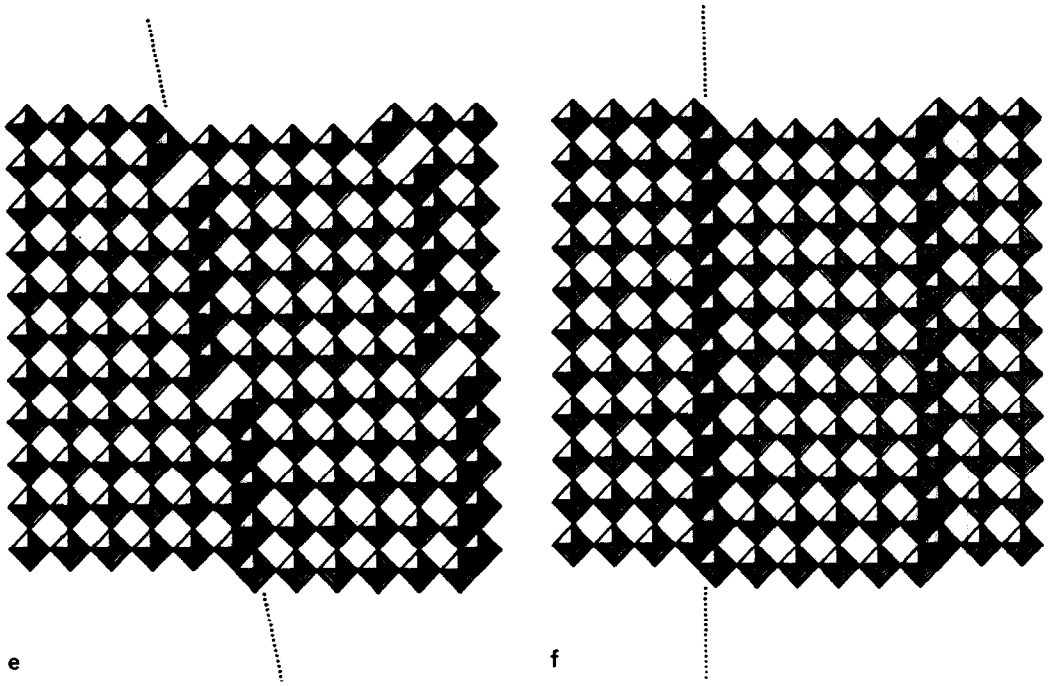

FIG. 1. Ideal structures with (a) APBs (101); and CS planes (b) (102), (c) (103), (d) (104), (e) (105) and (f) (001); all projected along [010]. They all have the same displacement vector $\frac{1}{2}[10\bar{1}]$. Octahedra share corners normal to the plane of the figure.

(102) CS planes. An indexed [010] zone axis diffraction pattern of the latter is given in Fig. 2.

5.2. $(Mo_{0.5}W_{0.5})O_{2.90}$

Various (102) CS structures M_nO_{3n-1} with $14 \leqslant \bar{n} \leqslant 18$ were observed. The diffraction spots were generally elongated parallel to g(102), so that only mean values $\bar{n}$ could be determined. Figure 3(a) shows $\bar{n} = 18$. Corresponding lattice fringe images such as Fig. 3(b) showed that D_{sp} was never constant over more than five adjacent CS planes.

The observed $\bar{n}$ values correspond to compositions $2.923 \leqslant \bar{x} \leqslant 2.944$; but we did not detect any compensating phase with $x < 2.90$, e.g., M_4O_{11} with $x = 2.75$, which would need to be present to the extent of about 18 mol % to give a mean composition $\bar{x} = 2.90$.

5.3. "$WO_{2.96}$"

In this sample (kindly provided some years ago by Dr. Ray Ackermann of the Argonne National Laboratory) most areas contained (103) CS structures. Parallel intergrowths of lamellae with different CS spacings occurred here also, which again made it difficult to get precise n values. The values measured from the diffraction patterns were $21 \lesssim n \lesssim 30$ $(2.905 \lesssim x \lesssim 2.933)$ with $n = 28 \pm 1$ predominating. A number of diffraction patterns suggested that adjacent phases have $\Delta n = 3$: the spots "sharpen up" at the strong reflections corresponding to the ReO_3 subcell, and one third and two thirds of the way between them, e.g., Fig. 4(a, b) [cf. also Fig. 2(a, b) of Ref. (*4*)]. Splitting of the spots on some patterns [e.g., Fig. 4(b)] may indicate swinging of the CS planes from (103) towards (104), or may be an effect of the monoclinic distortion of the ReO_3-type unit cell in WO_3 [discussed by Allpress and Gadó (*4*)].

5.4. "WO_3 (2)"

Some areas appeared to be unchanged WO_3: they were very prone to suffer beam damage [cf. ref. (*3*)]. Others contained {102} CS planes, in isolation or aggregated into small parallel groups (lamellae). The area in Fig. 5 showed four different orientations: (102), $(10\bar{2})$, (201) and $(20\bar{1})$. The mean D_{sp} of the group of five faults at A is approx 4.8 nm, corresponding to W_nO_{3n-1} with $n \approx 29$, i.e., $WO_{\sim 2.965}$. Other areas contained parallel {102} CS planes with spacings of 10 to 20 nm ($x = 2.983$–2.992), or with mean spacings of approx 3.7 nm but many faults, i.e., $\bar{n} \approx 22$, $\bar{x} \approx 2.95$. The mean composition was estimated to be roughly $x = 2.98$–2.99. Clearly the sample was very inhomogeneous.

TABLE II

SAMPLE PREPARATION CONDITIONS

Preparation	Starting materials	Tubes used	Temperature	Time	x
$MoO_{2.90}$	Mo + MoO_3 powders	evacuated quartz	1053 K	60 hr	2.90
$Mo_{0.5}W_{0.5}O_{2.90}$	Mo + MoO_3 + WO_3 powders	,, ,,	1073 K	48 hr	2.90
$WO_{2.96}$[a]	—	—	—	—	—
$WO_3(2)$	W + WO_3 powders	Pt, sealed in air	1373 K	36 hr	2.95
$WO_3(3)$	pellet of WO_3 powder	—	melted in Ar arc ($T_m \approx 1400$ K)	—	Black $WO_{3-\delta}$
$WO_3(5)$	W + WO_3 powders	Pt, sealed in air	melted at 1793 K, slow cooled to 1673 K, quenched in air to R.T.	2 min 1½ hr	2.95
$WO_3(6)$	W + WO_3 powder	,, ,,	melted at 1793 K, slow cooled to 1673 K, annealed *in vacuo* at 1273 K	2 min 1½ hr 24 hr	2.95
V_2MoO_8	V_2O_5 + MoO_3 powders	evacuated quartz	1073 K	3 days	2.667
$Nb_4(O,F)_{11}$	NbO_2F + Nb_3O_7F powders prepared as Ref. (*26*)	Pt, sealed in air	1273 K	8 days	2.750
$Nb_5(O,F)_{14}$	,, ,,	,, ,,	1043 K	10 days	2.800
$Nb_5(O,F)_{14}$	,, ,,	,, ,,	1273 K	8 days	2.800
$Nb_6(O,F)_{17}$	,, ,,	,, ,,	773 K	7 days	2.833
$Nb_6(O,F)_{17}$	,, ,,	,, ,,	1243 K	14 days	2.833
$Nb_8(O,F)_{23}$	,, ,,	,, ,,	1108 K	5 days	2.875
$Nb_{25}(O,F)_{74}$	,, ,,	,, ,,	1263 K	24 hr	2.96
$W_{0.9}V_{0.1}O_{2.95}$	WO_3 + V_2O_5 powders	,, ,,	963 K + 1573 K	24 hr 12 hr	2.95
$W_{0.9}Ta_{0.1}O_{2.95}$	WO_3 + Ta_2O_5	,, ,,	1573 K	26 hr	2.95
$W_{0.95}Nb_{0.05}O_{2.975}$	WO_3 + Nb_2O_5 powders	,, ,,	,,	48 hr	2.975
$W_{0.9}Nb_{0.1}O_{2.95}$	,, ,,	,, ,,	,,	26 hr	2.95
$W_{0.86}Nb_{0.13}O_{2.933}$	,, ,,	,, ,,	,,	26 hr	2.933
$W_{0.8}Nb_{0.2}O_{2.90}$	,, ,,	,, ,,	,,	48 hr	2.900

[a] Provided by Dr. R. J. Ackermann.

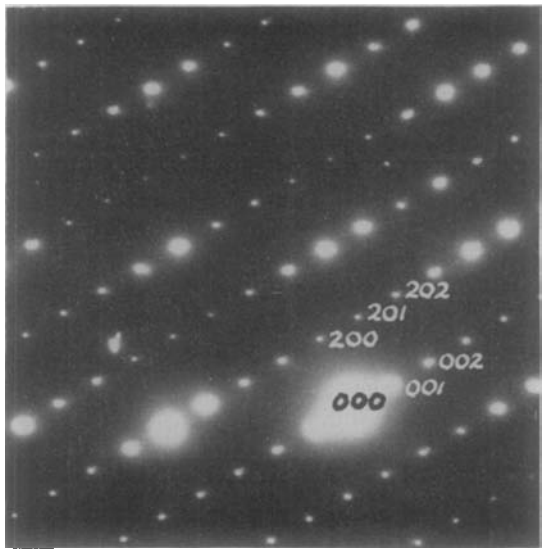

FIG. 2. (010) reciprocal lattice plane of Mo_9O_{26}. The indices correspond to the true unit cell (*16*).

Some diffraction patterns could not be indexed in terms of the reciprocal lattices of either WO_3 or (102) CS structures (cf. also Section 5.13).

5.5. "WO_3 (3)"

As expected for a quenched melt, both (102) and (103) CS structures were present, with a wide variation in n. Figure 6(a) shows heavy streaking parallel to g(102) with lighter streaks parallel to g(103).[3] Figure 6(b) indicates disordered (102) CS planes with a pronounced mean $\bar{n} \approx 14$, $\bar{x} \approx 2.92_9$.[4] Figure 6(c) shows (102) CS also with $\bar{n} \approx 14$ coexisting with (103) CS having $\bar{n} \approx 18$, $\bar{x} \approx 2.88_9$.[4] The

[3] Note also the obvious intermediate spots at $h + \frac{1}{2}$, 0, 0; 0, 0, $l + \frac{1}{2}$ and $h + \frac{1}{2}$, 0, $l + \frac{1}{2}$, presumably arising from the distortion of the ReO_3-type subcell, present in WO_3 and here.

[4] The intermediate spots are now absent. We presume the CS plane concentration is sufficiently high to prevent the tilting of $[WO_6]$ octahedra responsible for the subcell distortion in WO_3.

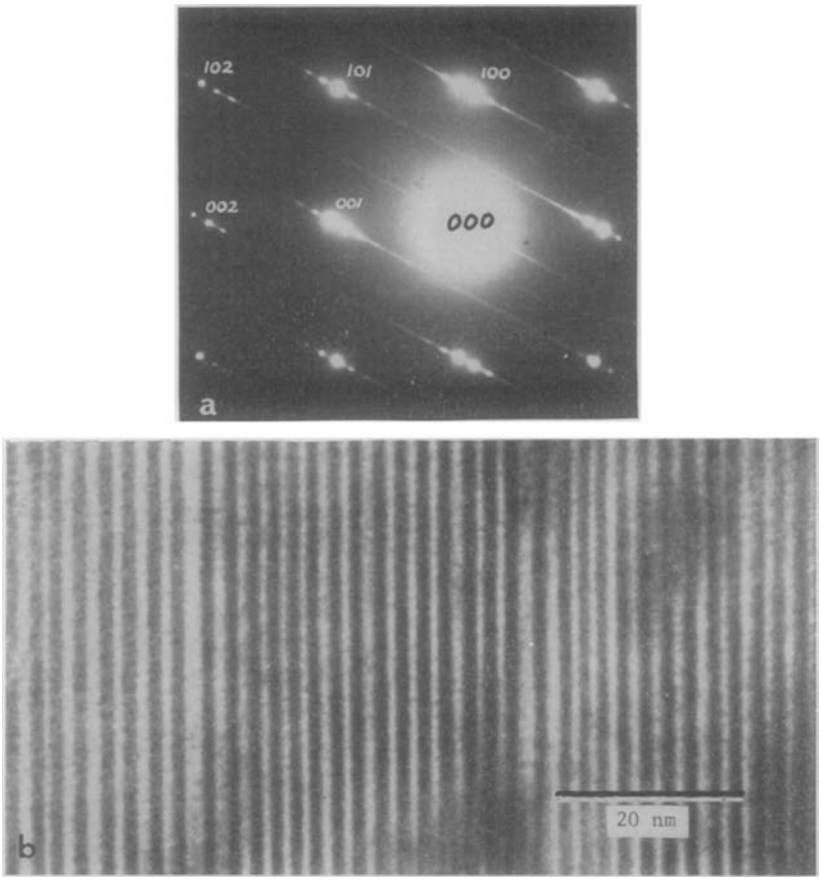

FIG. 3. (a) (102) CS with $\bar{n} = 18$ in $Mo_{0.50}W_{0.50}O_{2.90}$. (b) A lattice image from the same sample: note that the spacing of the CS planes, i.e., the dark fringes, is not constant over more than five adjacent CS planes.

total range of CS structures was (102) $14 \lesssim \bar{n} \lesssim 30$, (103) $13 \lesssim \bar{n} \lesssim 26$; respectively $2.92_9 \lesssim \bar{x} \lesssim 2.96_7$ and $2.84_6 \lesssim \bar{x} \lesssim 2.92_3$.

Figures 6(d, e) are a lattice image and the corresponding diffraction pattern with $\bar{n} \approx 24$ (103). In the former a not quite regular "superperiodicity" is apparent: a rather regular CS array is interrupted, often by a pair of closely spaced CS planes.

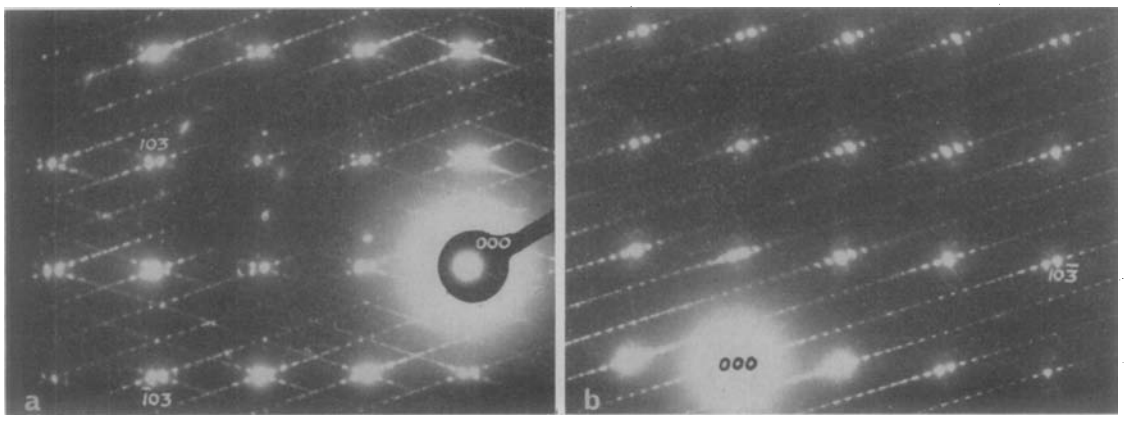

FIG. 4. (a, b) [010] zone of "$WO_{2.96}$," $\bar{n} = 28$. Several periodicities occur along g(103) and/or g(10$\bar{3}$). "Sharpening" of the spots at the strong subcell reflections and at one third and two thirds of the way along the rows strongly suggest that adjacent phases differ by $\Delta n = 3$.

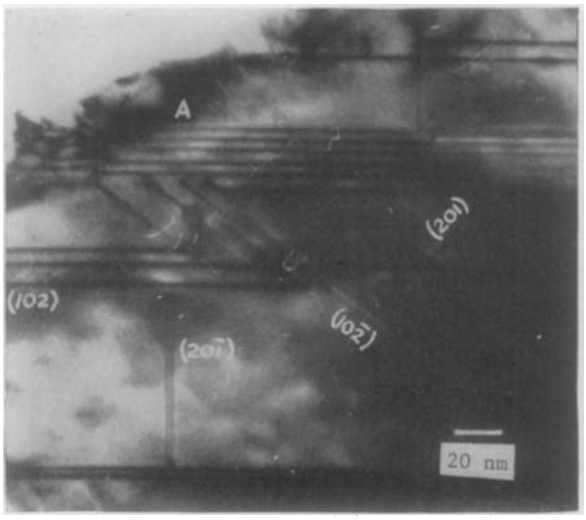

FIG. 5. (102), (10$\bar{2}$), (201) and (20$\bar{1}$) CS planes in WO_3(2). The mean D_{sp} of the group of five faults at A is approx. 4.8 nm corresponding to $WO_{\sim 2.965}$.

5.6. "WO_3 (5)"

CS was predominantly parallel to (103) with $\bar{n} \approx 15$ [Fig. 7(a)] or $\bar{n} \approx 29$ [Fig. 7(b)]. Intermediate values of n were not observed, but a relatively small proportion of (102) CS structures was also present.

5.7. "WO_3 (6)"

Mixtures of (102) and (103) CS structures again occurred, but with a reduced spread of n values: $\bar{n} = 26$ (103), $\bar{n} = 30$ (102) [Fig. 8(a, b)]. The lattice image in Fig. 8(c) was obtained using the reflections circled in Fig. 8(a): the dark fringes are parallel to (103), and their mean spacing corresponds to D_{sp} for $n = 27$ (measured 3.0_5 nm, calculated 3.0_8 nm for $n = 27$, 2.9_7 nm for $n = 26$). Superimposed on these are fine fringes which intersect the CS planes at intervals of 1.1_3 nm. Within the error of the magnification calibration this distance is equal to the a axis of the (103) CS structures, viz. 1.1_{86} nm. Note that these fine fringes change direction

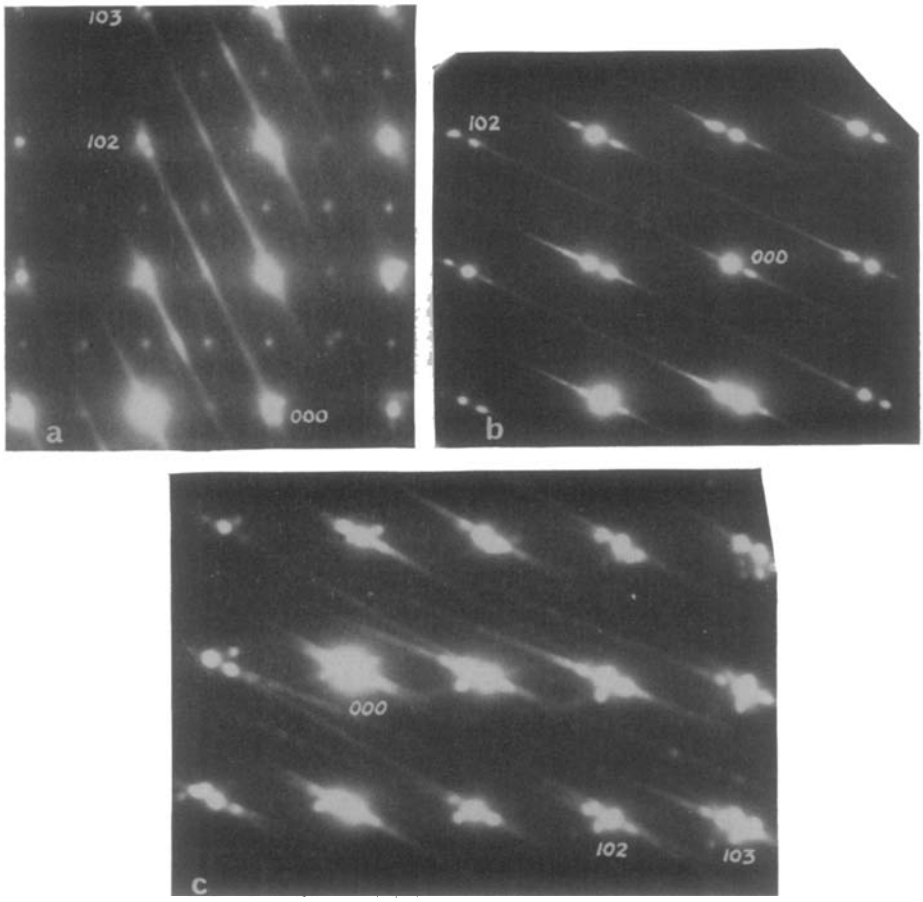

FIG. 6. a to c.

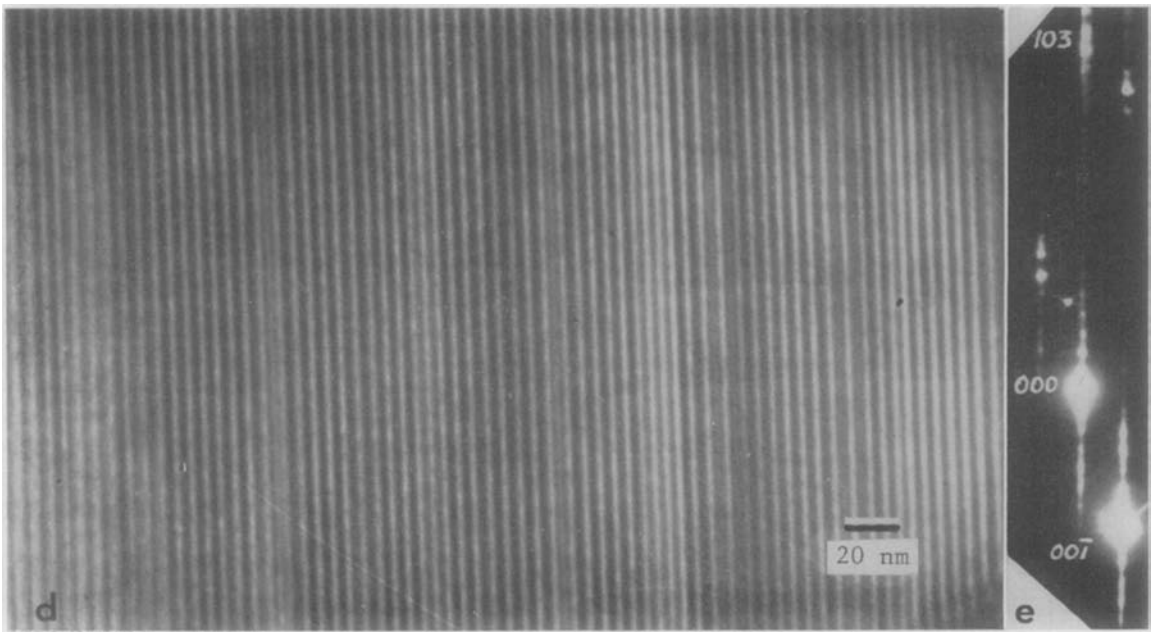

FIG. 6. WO_3(3). (a) Intense streaking parallel to **g**(102), and faint streaking along **g**(103). Note the intermediate spots at $h+\frac{1}{2}, 0, l$ and, especially, $h, 0, l+\frac{1}{2}$ and $h+\frac{1}{2}, 0, l+\frac{1}{2}$: these also appear in the diffraction patterns from some of the polymorphs of pure WO_3. (b) indicates disordered (102) CS planes with a pronounced mean spacing corresponding to $\bar{n}=14$, i.e. $\bar{x}\approx 2.929$. The intermediate spots are now absent. (c) (102) CS with $\bar{n}\approx 14$ coexisting with (103) CS having $\bar{n}\approx 18$ ($\bar{x}\approx 2.857$ and 2.889, respectively). The intermediate spots are again absent. (d, e) Lattice image and corresponding diffraction pattern (rotated approx $\pi/2$) with $\bar{n}\approx 24$ (103). A not quite regular "superperiodicity" is apparent in d; the rather regular CS array being interrupted, often by a pair of closely spaced CS planes.

whenever the CS plane spacing varies. (This is clear if the micrograph is viewed at grazing incidence along the direction of the fine fringes.)

5.8. V_2MoO_8

CS was parallel to (001) with mainly $n=3$ [Fig. 9(a)], i.e., the Nb_3O_7F structure type. The specimens were very well ordered, and only a low density of (001) faults occurred [Fig. 9(b)]. Also present was a relatively small amount of $n=2$ (001), i.e., the V_2O_5 structure type [Fig. 9(c)], which also contained a low density of (001) = $(100)_{V_2O_5}$ faults [see Fig. 9(d)], and very faint streaking along $\pm\mathbf{g}(h00)_{V_2O_5}$ in Fig. 9(c).

5.9. $NbO_2F + Nb_3O_7F$

Apart from crystal growth by vapour transport the reactants remained unchanged: ReO_3-type NbO_2F and $n=3$ (001), i.e., Nb_3O_7F. No other n values were observed.

5.10. $W_{0.9}V_{0.1}O_{2.95}$

No long-period CS structures were detected: the diffraction patterns corresponded to WO_3 and a structure similar to the V_2O_5 type. The diffraction pattern of the latter is shown in Fig. 10(a), which should be compared with Fig. 9(c). Virtually continuous streaking parallel to $a^*_{V_2O_5}$ shows that the V_2O_5 b axis must be doubled. Kihlborg and Israelsson (*15*) have discussed similar streaking in X-ray diffraction patterns from $(W_{0.375}V_{0.625})_2O_5$; it is believed to result from imperfect ordering of W and V.

5.11. $W_{0.9}Ta_{0.1}O_{2.95}$

Some (103) CS was present, as is shown in Fig. 10(b) where $\bar{n}\approx 40$; but the specimens were of poor quality and not monophasic. In the same figure streaking parallel to $\mathbf{g}(10\bar{3})$, **g**(301) and possibly **g**(001) and **g**(104) also appears.

Gadó and Magnéli (*13*) reported that $W_{35}Ta_4O_{115}$ could be prepared in quartz glass tubes at 1473 K. We found that, at 1373 K, quartz tubes were severely damaged and the products were markedly different in both colour and crystallinity from those prepared in Pt at 1573 K.

5.12. $W_{0.95}Nb_{0.05}O_{2.975}$

No long-period CS structures were found. The product was inhomogeneous, and the phases present were not identified.

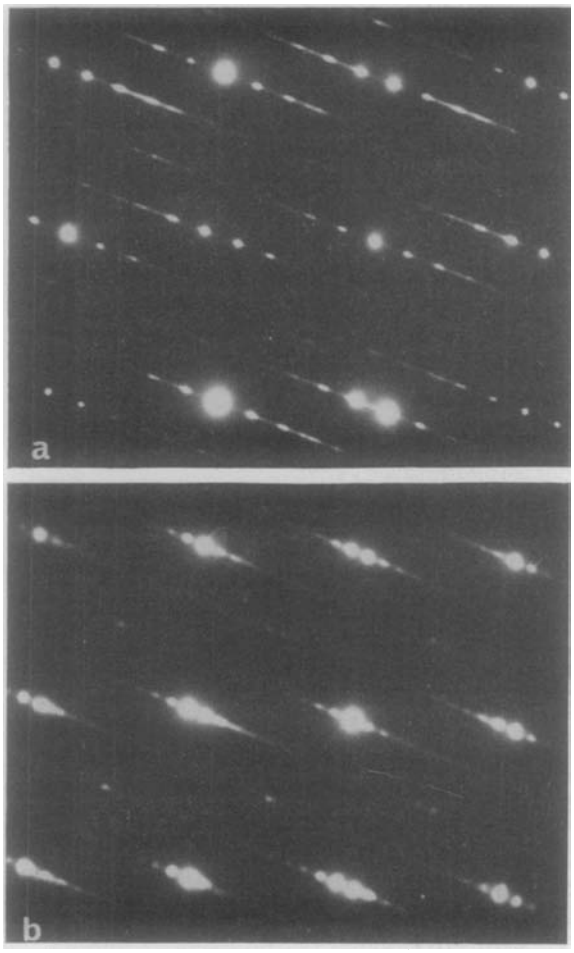

FIG. 7. WO_3(5). (103) CS with $\bar{n} = 15$ (a), and $\bar{n} = 29$ (b).

5.13. $W_{0.9}Nb_{0.1}O_{2.95}$

Long-period superstructures were present; Fig. 11(a) implies (104) CS planes with a small range of composition about $\bar{n} \approx 63$, i.e., $\bar{x} \approx 2.952$. The marked "sharpening" of the spots, not only near the strong ReO_3 subcell reflections but also at the positions $(h + m/4)$, 0, l with $m = 1$, 2 or 3, strongly suggests that adjacent phases differ by $\Delta n = 4$.

Figure 11(b) shows the corresponding lattice image. Although the fringe spacing is uniform many types of defect are present: a cooperative wave-like inflection in the direction of several CS planes with no strain contrast at A; slight change in the fringe direction at B; and strong strain contrast which is sometimes, e.g., at C, but not always, e.g. at D, associated with the termination of a CS plane inside the crystal.

Some areas showed a quite different type of unidentified WO_3 superlattice pattern (cf. also Section 5.4).

5.14. $W_{0.867}Nb_{0.133}O_{2.933}$

CS parallel to $(10\bar{4})$, (104), approx (105) and $(10\bar{5})$, and (001) all occurred, often in the same flake [Fig. 12(a)]. The values of n were 56 and 60 {104}, 70 and 75 {105}, and 15 and 16 (001); i.e., $\bar{x} = 2.952$, 2.948 and 2.935. The coincidences of diffraction spots indicate $\Delta n = 4$ between adjacent {104} CS structures and $\Delta n = 5$ between adjacent {105} CS phases. Figure 12(b) shows coexisting {104} and {105} CS more clearly. Figure 12(c) is a lattice image corresponding to Fig. 12(a): the cooperative behaviour of the CS planes is very striking, e.g., in subtle changes in orientation from (104) to (105) as well as in sharper but still coherent reorientation to (001). These last CS planes are usually "stepped", consisting of relatively long (001) segments joined by possibly (105) sections. Often the steps are well ordered over areas of about 10^3 nm^2 (e.g. at X, approx 2×10^3 nm^2) giving regions with very high values of p. Sometimes a row of steps extends over many tens of CS planes (e.g., at Y). Cooperative inflections and strain contrast are again visible.

Figure 12(d) is a diffraction contrast image of (104) CS planes slightly inclined to the electron beam. Across the picture there is change in the CS plane spacing that varies with distance from the edge of the crystal. The spacing is fairly uniform at the edge and well away from it, though it is slightly different at these two positions. The insertion of the "extra half-plane" of CS produces a complex cooperative "stepping" of the neighbouring CS planes.

5.15. $W_{0.8}Nb_{0.2}O_{2.90}$

Again long-period superstructures were absent. Different types of superstructure based on the WO_3 subcell were again observed, but not identified.

6. Discussion

6.1. $MoO_{2.90}$ and $Mo_{0.5}W_{0.5}O_{2.90}$

Our observations confirm that Mo_9O_{26} is the highest stable pure molybdenum oxide with (102) CS, coexisting with MoO_3 at 1053 K.

$Mo_{0.5}W_{0.5}O_{2.90}$ contained (102) CS phases M_nO_{3n-1} with $14 \leqslant \bar{n} \leqslant 18$ ($2.929 \leqslant \bar{x} \leqslant 2.944$), as deduced by Magnéli et al. (*16*). The difficulty experienced by these authors in identifying $\bar{n} \geqslant 14$ is explained by the lattice image in Fig. 3(b): all these n values occur, but there is no long range ordering.

There was no evidence to support the hypothesis that the CS planes rotate from (102) towards (103); and the apparent absence of a compensating phase

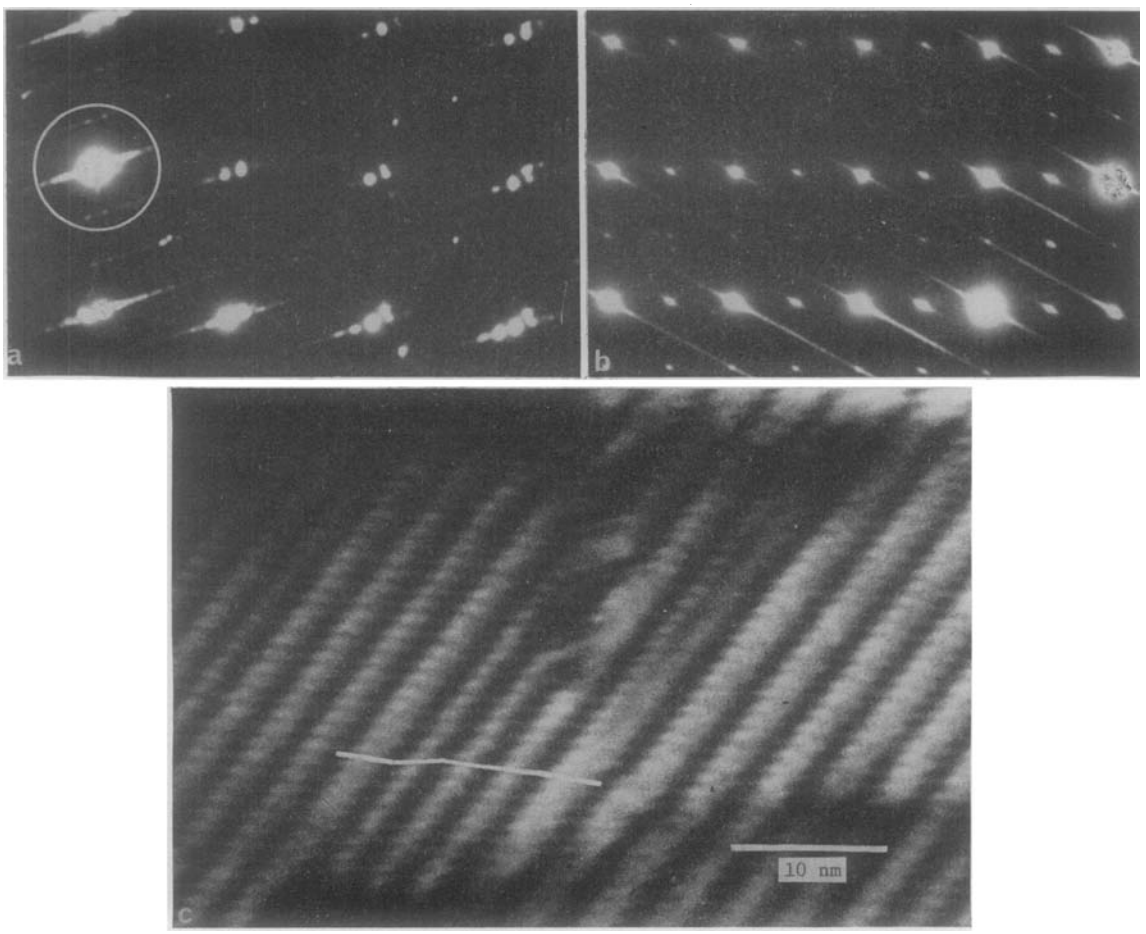

FIG. 8. WO_3(6). Diffraction patterns from CS structures with (a) $\bar{n} = 26$ (103) and (b) $\bar{n} = 30$ (102). (c) The lattice image obtained using the reflections circled in (a). The broad dark fringes are CS planes parallel to (103) with $D_{sp} = 3.05$ nm, i.e., $n = 27$. Superimposed on these are fine fringes parallel to **c** or **a** + **c** of the CS structure (true cells). The fine fringes intersect the CS planes at intervals of $a = [103]_{ReO_3}$. Note how they change direction as the CS plane spacing varies. (View at grazing, angle along the fine fringes.) Note also the extra half-plane of CS, and the way in which it is accommodated by cooperative stepping of adjacent CS planes [cf. Fig. 12(d)].

with $x < 2.90$, both in our work and that of Magnéli et al., remains a puzzle.

6.2. WO_x

We confirm Tilley's finding (*3*) that (102) CS planes occur when x is close to 3.0 and that, as x decreases, they aggregate into lamellae, eventually forming macroscopic domains of almost ordered (102) CS structures. [In these respects slightly reduced WO_3 closely resembles slightly reduced rutile (*17*).] The lamellae have $\bar{x} \approx 2.97$ (cf. 1.98 in reduced rutile) which suggests that the highest ordered (102) CS structure has $n \approx 30$ ($W_{30}O_{89} = WO_{2.96}$). The lowest (102) structure observed was $\bar{n} \approx 14$ ($\bar{x} \approx 2.929$) in a quenched melt: it coexisted with $\bar{n} \approx 18$ (103) ($\bar{x} \approx 2.889$). After this sample had been annealed at 1273 K the lowest (102) phase was $\bar{n} \approx 30$ ($\bar{x} \approx 2.96\dot{}$) and it coexisted with $\bar{n} \approx 26$ (103) ($\bar{x} \approx 2.923$). These observations indicate that the (102) CS family is stable to lower compositions at higher temperatures. Again this parallels the observations on the $p = 1$ family in the titanium oxide system (*10*).

Well-ordered (102) CS structures were never observed. It would appear that the minimum concentration of (102) CS planes required to form a stable aggregate is very close to the maximum concentration—at which composition (103) CS planes are more stable. The relatively high degree of reduction in the aggregate/lamella as compared with that in reduced rutile ($WO_{3-\delta}$ with $\delta \approx 0.03$; $TiO_{2-\delta}$ with $\delta \approx 0.02$) reflects the differences

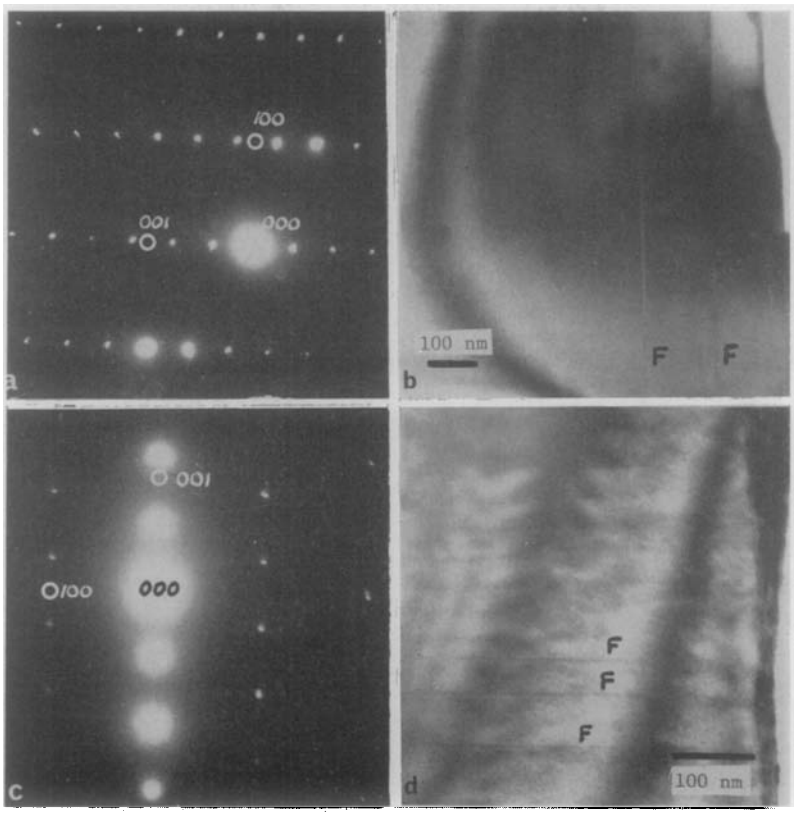

FIG. 9. (a) Diffraction pattern of V_2MoO_8, a (001) CS structure with $\bar{n} = 3$ (ReO_3 indices). The specimens are very well ordered with only a low density of (001) faults F, seen in (b). (c) Diffraction pattern of V_2O_5 type [$n = 2$ (001)] with very faint streaking along $\mathbf{g}(001)_{ReO_3} = \mathbf{g}(100)_{V_2O_5}$. These specimens also had a very low density of faults parallel to (001), as shown in (d).

between the ReO_3- and rutile-type structures. The maximum stable CS plane spacings are remarkably similar: 4.8 nm for the group of five faults in Fig. 5 compared with 4.9 nm for a group of six faults in $TiO_{2-\delta}$ [Fig. 1(c) in Ref. (*17*)].

It is apparent that Gebert and Ackermann (*2*) correctly identified the CS plane as (103), and their choice of $n = 25$ in W_nO_{3n-2} (the ideal value before doubling the c axis and inserting the interstitial oxygen) is entirely compatible with our observa-

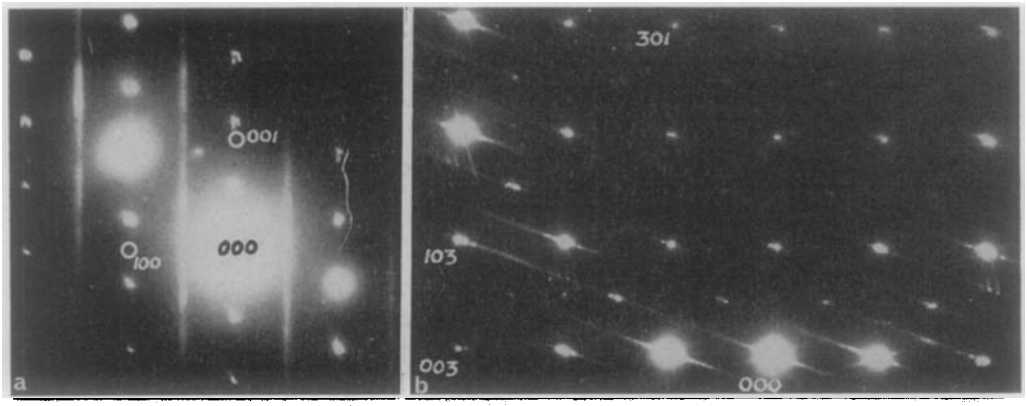

FIG. 10. (a) Diffraction pattern of $W_{0.9}V_{0.1}O_{2.95}$ showing the presence of the V_2O_5-structure type [cf. Fig. 9(c)]. The position of the continuous streaks parallel to $\mathbf{a}^*_{V_2O_5}$ shows that the V_2O_5-type **b** axis ($= \mathbf{a}_{ReO_3}$) must be doubled, cf. Ref. (*15*). (b) (103) CS with $\bar{n} \approx 40$ in $W_{0.9}Ta_{0.1}O_{2.95}$. The diffraction pattern also shows the presence of CS parallel to $(10\bar{3})$, (301), and possibly (001) and (104).

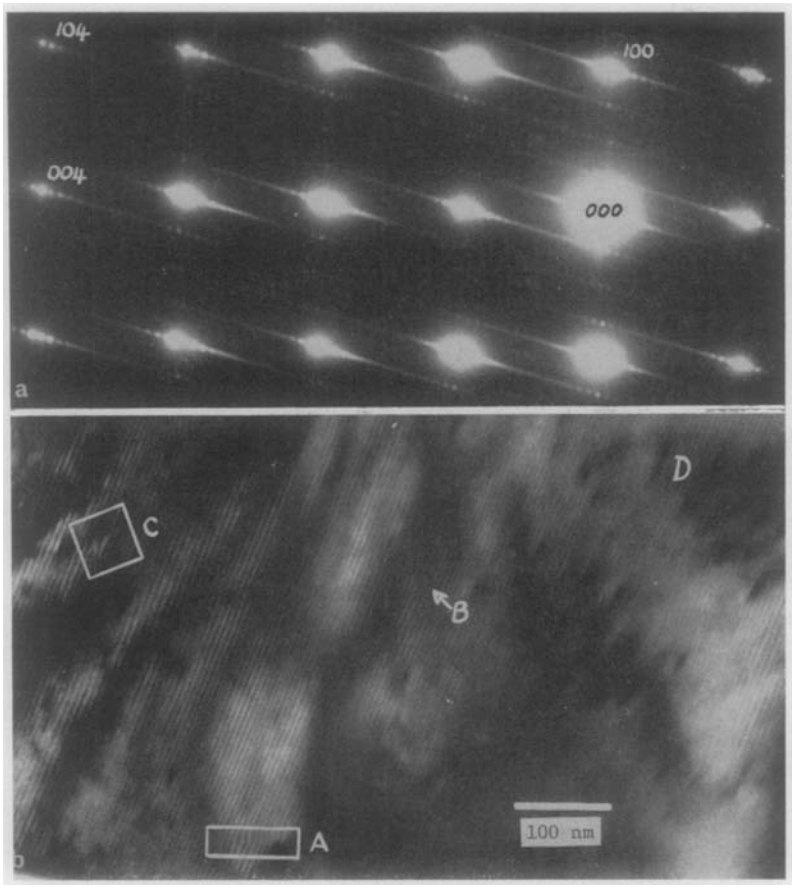

FIG. 11. (a) (104) CS with $n \approx 63$ in $W_{0.9}Nb_{0.1}O_{2.95}$. Sharpening of the spots at $(h + m/4)$, 0, l with $m = 1, 2, 3$ suggests $\Delta n = 4$. (b) Lattice image of (a): by and large the fringe spacing is very regular, but note the various defects at A, B, C, D referred to in the text).

tions, which revealed $21 \leqslant n \leqslant 30$, but mainly $n = 28$. Observations on our sample WO_3(6) (Section 5.7) show that, even in a well-annealed sample, every single crystal does not necessarily have the same composition: we found comparable amounts of $WO_{2.97}$ (102) and $WO_{2.93}$ (103) coexisting in the same preparation. [This suggests that the equilibrium partial molar free energy of oxygen is virtually independent of composition in this composition range, as Marucco, Gerdanian and Dodé (*18*) have indeed observed at 1273 K.] We therefore believe that it is not necessary to insert the extra interstitial oxygen into the (103) CS structure of ideal stoichiometry $W_{25}O_{73}$. Accepting Magnéli's structure for $W_{20}O_{58}$ and the structural principle for the (103) CS family W_nO_{3n-2} forces us to the same conclusion.

The existence of $n = 40$ (103), i.e., the phase $W_{40}O_{118}$ reported by Gadó and Magnéli (*13*), must also be questioned. We did not find $n > 30$ (103); indeed, the composition and preparation temperature given by these authors lie well inside the (102) CS phase field of WO_x delineated by our observations.

6.3. V_2MoO_8 and $NbO_2F + Nb_3O_7F$

The observations on these specimens are entirely consistent with the earlier X-ray diffraction results (*26*, *27*). We were not able to detect $n > 3$. A very low density of (001) faults was observed in V_2MoO_8 and NbO_2F, and also in $(V_{1-a}Mo_a)_2O_5$.

6.4. The Pseudobinary Systems $WO_3 + M_2O_5$ (M = Ta, Nb, V)

At $x = 2.95$ the CS plane was (103) for M = Ta and (104) for M = Nb. V_2O_5 did not react with WO_3 to form long-period CS structures, and perhaps this may be formally described as a diphasic gap between $n = 2$ (001) ($= V_2O_5$) and $n = \infty$, i.e., WO_3.

For $x = 2.933$ and M = Nb (i.e., $Nb_2O_5 \cdot 13WO_3$) at least three types of CS structure coexisted with coherent boundaries: (104), (105) and (001). Thus $p = 3, 4, \infty$ ($q = 1$) all have very similar stabilities at $x = 2.933$, but (104) is the most stable at higher compositions.

A more detailed "phase analysis" of these pseudobinary systems is clearly needed. Our results on $WO_3 + Nb_2O_5$ are broadly consistent with Roth and Waring's interpretation of their X-ray diffraction observations on the same system for samples prepared at the same temperature, 1573 K (*12*). The inconclusive nature of these authors' interpretations is quite understandable in the light of our data. X-Ray diffraction methods are not sufficiently incisive; and the subtle textures we observe cannot be accommodated in a conventional phase diagram. [Cf. the discussion in Ref. (*19*).]

6.5. Defects and Reaction Mechanisms

Parallel intergrowths of different n values frequently occur. This is shown by the spread in D_{sp} observed in both diffraction patterns [Figs. 3(a), 4(a), 6(b), 7, 8(a, b), 11(a)] and lattice images [Figs. 3(b), 8(c)]. Usually the intergrowth is more or less random but occasionally [Fig. 6(d)] there is a suggestion of ordering.

A detailed interpretation of fringe patterns [such as Fig. 8(c)] will be published elsewhere; here we will give only a brief summary. There is a one-to-one correspondence between the fine fringes and the **c** axis (sometimes **a** + **c**) of the (103) CS structures. Thus the fine fringes provide an extremely sensitive means of measuring changes in n.

Steps in and cooperative bending of CS planes, strain contrast, and dislocations in the CS plane lattice occurred frequently in the WO_x and $(W,Nb)O_x$ systems [Figs. 11(b), 12(c, d)]. These "defect complexes" shed light on the mechanism by which the composition changes. Usually, the composition of a preparation will fall in a "two-phase region": at least two adjacent phases will coexist as an intimate parallel intergrowth. Lateral cooperative diffusion of an additional CS plane into the crystal from the surface [the Andersson–Wadsley mechanism (*20*) but see also Ref. (*28*)] can only occur at that very small proportion of the surface which is parallel to the CS planes. More likely (even on purely statistical grounds) is the insertion of a new CS plane between those already

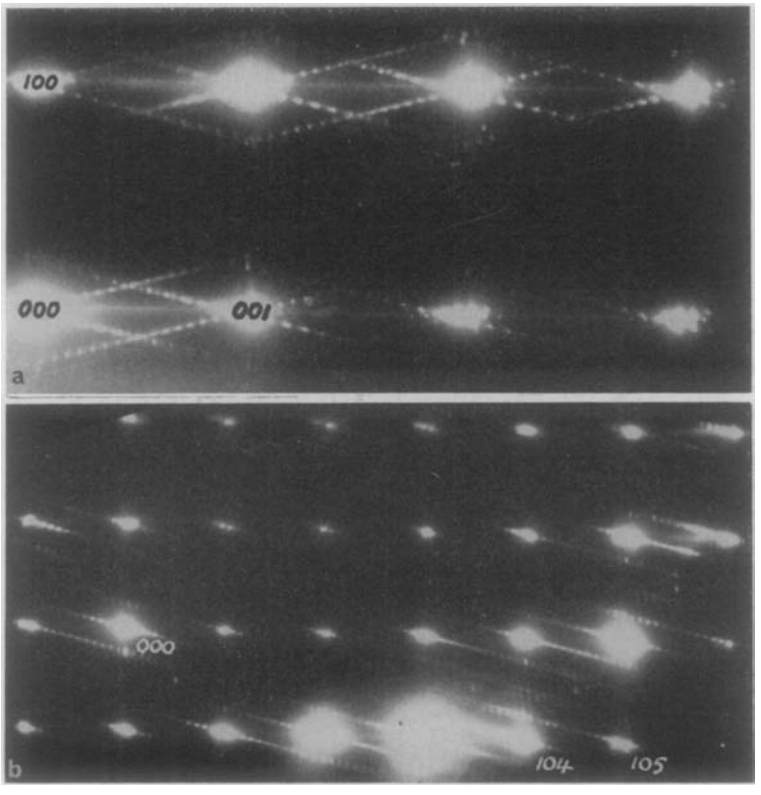

FIG. 12 a and b.

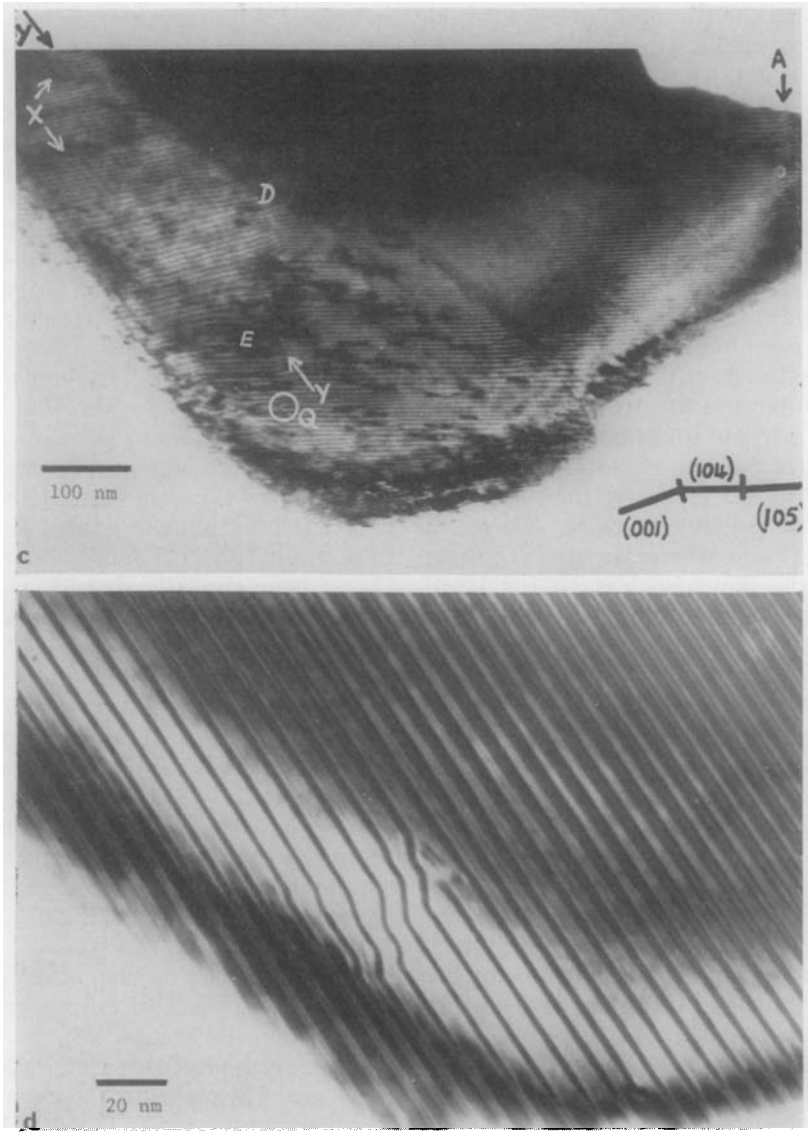

FIG. 12. $W_{0.867}Nb_{0.133}O_{2.933}$. (a) Diffraction pattern showing CS parallel to (104), (10$\bar{4}$), (001) and approx (105), (10$\bar{5}$). The n values are 56, 60 {104}, 15, 16 (001) and 70, 75 {105}. (b) A clearer indication of coexisting (104) and (105) CS. (c) Lattice image corresponding to (a): notice the stepped CS planes at X, a long row of steps aligned along YY, cooperative inflections in the CS planes at A, and a (104) CS plane terminating at Q. In the large region of well-ordered CS planes from the centre to the right of this picture their direction changes from (104) to (105) and back to (104), a range of 2.7° ≈ 0.05 rad: this is most obvious if the picture is viewed approx along the CS plane direction at grazing incidence. The dark lines, e.g., around E, appear to be dislocations lying approximately in the plane of the figure. Most do not appear to interact with CS planes but some do (D). (d) An extra half CS plane inserted into a fairly regular array. Note the cooperative stepping of adjacent CS planes to the left which distributes the composition and elastic stress over a relatively large volume.

in existence, at some point either on the surface or inside the crystal. This is accommodated by the thrusting aside of neighbouring CS planes (laterally, by the Andersson–Wadsley mechanism) in exactly the way displayed in Fig. 12(d). Thus a dislocation is generated in the CS plane lattice; a superdislocation in the sublattice. Various stages in this process appear in Figs. 11(b), 12(c, d) and 8(c). This is a logical development of the dislocation mechanism previously proposed (*8, 9*). The diffusion mechanism (*20*) is responsible for the ripples or steps which appear on the CS planes, and which minimize both

the elastic stress and the composition stress of the CS dislocation by distributing them over a relatively large volume of crystal. Thus there are no severe local deviations in stoichiometry. (In contrast, direct insertion or removal of a CS plane without such accommodation would produce lamellae of stoichiometry $m = n/2$ or $2n$.)

The strain contrast [Figs. 11(b), 12(c)] suggests that nucleation of new CS planes may occur *inside* the crystal; that it is not necessarily restricted to the surface. Strain contrast would be expected at a "vacancy cluster" prior to its collapse into a nucleus of CS plane bounded by a dislocation loop, and certainly it would be present at the nucleus after the collapse. In this regard it seems to us significant that at some points showing strain contrast [e.g., D in Fig. 11(b)] the CS planes in the immediate neighbourhood are slightly buckled; they are starting to be thrust aside: whereas no strain contrast is visible at some other points [such as Q in Fig. 12(c)] where a CS plane ends inside the crystal.

Figures 11(b) and 12(c) show that the CS planes may change orientation coherently, without any sharp boundary. We saw earlier (Section 2) that a variation in direction along a CS plane changes the proportions of CS and APB components. The same elementary diffusion steps, that in the Andersson Wadsley mechanism (*20*) allow a CS plane to migrate sideways, may be utilized to explain how it changes orientation: each jump of $\frac{1}{2}\langle 101\rangle$ converts a CS unit into an APB unit,[5] or vice versa. In this way [MO] units may be transported along the plane, changing the ratio p/q and the orientation of the CS plane, and introducing a composition change in the crystal. This mechanism will be discussed in more detail elsewhere.

6.6. General Comments

6.6.1. In a preliminary paper on the systems TiO_x and $(Ti,Cr)O_x$ (*10*) we reported the CS planes

$$(hkl)_r = p\cdot(121)_r + q\cdot(011)_r,$$

and stated that $q = 1$ "is at least predominant."[6] Subsequent study has revealed a number of instances in which $q > 1$, so that a virtually continuous "swing" of the CS planes between $(121)_r$ and $(132)_r$ is possible.

The behaviour observed in the present study is much simpler: most diffraction patterns yield $q = 1$, i.e., only $(10l)$ CS planes are unequivocally identified, and these are relatively few, *viz.* $p = 1, 2, 3, 4, \infty$. [However, the stepped CS planes in Fig. 12(c) could be described as having $p \gg 4$.]

There is some suggestion (*16*) that, for higher n values, the (102) M_nO_{3n-1} structures are only stable for even n; i.e. between adjacent phases $\Delta n = 2$ [cf. $(132)_r$ Ti_nO_{2n-1} (*21*)]. Similarly, many of our diffraction patterns suggest that $\Delta n = 3$ for (103) M_nO_{3n-2}, $\Delta n = 4$ for (104) M_nO_{3n-3} and, possibly, $\Delta n = 5$ for (105) M_nO_{3n-4}. If these suggestions are confirmed by subsequent study their origin may be expected to lie in the structures. Figure 1 shows that in a given $(10l)$ CS family all phases for which $\Delta n = l$ have similarly shaped columns of corner-sharing $[MO_6]$ octahedra (united at CS planes). If n/l is an integer all the strings of corner-shared octahedra in a given direction ($\langle 100\rangle$ or $\langle 001\rangle$) are the same length, n in one direction and n/l in the other. If, by the diffusion mechanism (*20*) for changing n, *each* CS step moves a unit jump in unison then $\Delta n = 2, 3, 4$, etc., for (102), (103), (104), etc., respectively. These intervals in n (suggested by the diffraction evidence) are therefore compatible with the mechanism for moving CS planes so as to change the composition. (If $\Delta n = 1$, only 1 in every l CS steps will jump.)

Further, precise measurements of n are required, perhaps using the lattice fringe-imaging technique [cf. Fig. 8(c) and Section 6.5].

6.6.2. In the ReO_3-derived structures considered here, the CS plane is the favoured method of accommodating excess cations. Magnéli has discussed some reasons for this (*11*): fundamentally, the APB component of the CS plane allows an interstitial [MO] unit to be inserted into the structure with a minimum amount of edge sharing between octahedra (*28*). If no APB were present a single interstitial [MO] row would produce clusters of five edge-sharing octahedra, the centre one having all its edges in the (010) plane shared with neighbouring octahedra. Edge sharing is obviously associated with an energy increase (and we may note that pairs of edge-shared octahedra occur even in an APB).

The concentration of CS steps is determined by the stoichiometry of the crystal: the problem is how to distribute them so as to minimize the energy. (The configurational entropy of CS planes is

[5] A CS unit or step is a pair of edge-shared octahedra joined to adjacent octahedra by edge-sharing. The APB unit or "step" consists of the two terminal octahedra of the edge-shared strip in the CS plane: each shares only *one* edge with neighbouring octahedra.

[6] In that paper we used a and b for p and q. The change to the latter pair is desirable for subsequent discussions (D. K. Philp, to be published) in order to avoid confusion with unit cell vectors **a**, **b**. They are not the same as the parameters p and q used by Magnéli (*1*).

negligible.) We may formally resolve the energy of a CS structure into two terms, due to two sets of interactions between the CS steps: those within a CS plane, and those between CS planes. The observations reported above show that, in a given system, the CS steps are most widely separated by APB steps when the CS planes are most widely spaced; i.e., when they are "isolated." This implies repulsive interaction between the CS steps in a plane (the first of the two energy terms). Its magnitude decreases in the sequence Mo > W > Ta > Nb, since l in ($h0l$) *increases* in the same order. This is further explained by Fig. 13: the energy per CS step decreases with increasing separation; but increasing separation means increasing numbers of APB steps, and the energy due to these must therefore increase simultaneously. If these energies increase at a rate faster than linear with increasing density (decreasing separation) then the total energy per CS step will pass through a minimum as p/q changes from zero to infinity, i.e., as the CS plane swings from (101) to (001). This is shown schematically in the figure, which also shows that if the APB energy term is assumed to be constant (for a given p/q) the minimum shifts to higher p [higher l in ($h0l$)] as the CS energy term decreases.

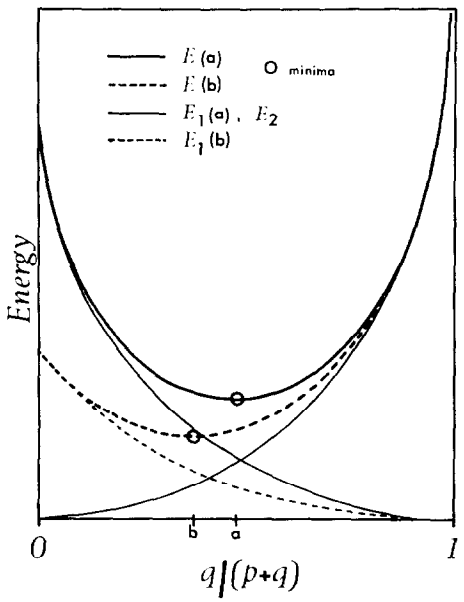

FIG. 13. A schematic diagram to show how the energy per CS step (i.e., per oxygen eliminated) varies with the orientation of the CS plane ($h0l$) = p(001) + q(101). [(001) is the CS part and (101) the APB part.] The total energy E is resolved into 2 components: E_1 due to the CS step and E_2 due to the APB part. ($E_2 = q/p \times$ the energy per APB step.) The stable CS plane is given by the value of $q/(p+q)$ at the minimum total energy. E_1 is assumed to vary with the cation M in $(M^{5+},W^{6+})O_{3-\delta}$. The two cases **a** and **b** have $E_1(\mathbf{a}) > E_1(\mathbf{b})$, so that at the minima $q_\mathbf{a}/p_\mathbf{a} > q_\mathbf{b}/p_\mathbf{b}$.

Between adjacent CS planes there must be an attractive interaction when D_{sp} is large, otherwise we would not observe aggregation into lamellae. As D_{sp} decreases, i.e., for a given CS plane as x decreases, so this interaction becomes repulsive also. [This is the second of the energy terms introduced above; cf. Ref. (*17*).] Thereafter, as x decreases still further, the optimum CS plane (10l) will be determined by a balance between intra- and inter-CS plane interactions. As inter-CS plane repulsion becomes stronger the proportion of APB component will fall, i.e., p/q will increase, l in ($h0l$) will increase, and the strips of edge-shared octahedra will become longer. This is because, for a fixed composition, an increase in p/q (which increases the first energy term) produces a higher oxygen defect at each CS plane, and therefore allows a larger D_{sp} (and a lower second-energy term).

Temperature is also a determining factor. The observations on WO_x (Section 6.2) show that p/q decreases as the temperature increases, so that the minimum p persists to lower compositions. This suggests that the cation radius ratio r_{5+}/r_{6+} may be a controlling factor: this will decrease as the temperature increases, and presumably also in the sequence $Nb^{5+} > Ta^{5+} > W^{5+} > Mo^{5+}$.

7. Acknowledgments

We are grateful for financial support from the Australian Research Grants Committee, and for Grant No. AFOSR-69-1806 from the Office of Scientific Research of the United States Air Force. Our thanks also go to Dr. L. N. D. Lucas, Mr. M. K. Holmes and the other staff for facilities provided at the Electron Microscopy Centre of this University, and to Miss R. Coroneos for preparing some of the niobium oxyfluoride samples.

8. References

1. A. MAGNÉLI, *Acta Cryst.* **6**, 495 (1953).
2. E. GEBERT AND R. J. ACKERMANN, *Inorg. Chem.* **5**, 136 (1966).
3. R. J. D. TILLEY, *Mat. Res. Bull.* **5**, 813 (1970).
4. J. G. ALLPRESS AND P. GADÓ, *Cryst. Lattice Defects* **1**, 331 (1970).
5. J. SPYRIDELIS, P. DELAVIGNETTE, AND S. AMELINCKX, *Mat. Res. Bull.* **2**, 615 (1967).
6. S. AMELINCKX AND J. VAN LANDUYT, "The Chemistry of Extended Defects in Non-metallic Solids," (L. Eyring and M. O'Keeffe, Eds.), p. 295, North-Holland, Amsterdam, 1970.

7. L. A. BURSILL AND B. G. HYDE, *Phil. Mag.* **20**, 657 (1969).
8. J. S. ANDERSON AND B. G. HYDE, *Bull. Soc. Chim. Fr.* 1215 (1965).
9. J. S. ANDERSON AND B. G. HYDE, *J. Phys. Chem. Solids* **28**, 1393 (1967).
10. L. A. BURSILL, B. G. HYDE, AND D. K. PHILP, *Phil. Mag.* **23**, 1501 (1971).
11. A. MAGNÉLI, *Arkiv Kemi* **1**, 513 (1949).
12. R. S. ROTH AND J. L. WARING, *J. Res. Nat. Bur. Stand.* **70A**, 281 (1966).
13. P. GADÓ AND A. MAGNÉLI, *Mat. Res. Bull.* **1**, 33 (1966).
14. B. G. HYDE AND L. A. BURSILL, "The Chemistry of Extended Defects in Non-metallic Solids," (L. Eyring and M. O'Keeffe, Eds.), p. 347, North-Holland, Amsterdam, 1970.
15. L. KIHLBORG AND M. ISRAELSSON, *Acta Chem. Scand.* **22**, 1685 (1968).
16. A. MAGNÉLI, B. BLOMBERG-HANSSON, L. KIHLBORG, AND G. SUNDKVIST, *Acta Chem. Scand.* **9**, 1382 (1955).
17. L. A. BURSILL AND B. G. HYDE, *Phil. Mag.* **23**, 3 (1970).
18. J.-F. MARUCCO, P. GERDANIAN, AND M. DODÉ, *J. Chim. Phys.* **66**, 674 (1969).
19. "The Chemistry of Extended Defects in Non-metallic Solids," (L. Eyring and M. O'Keeffe, Eds.), Discussion, p. 651, North-Holland, Amsterdam, 1970.
20. S. ANDERSSON AND A. D. WADSLEY, *Nature* **211**, 581 (1966).
21. L. A. BURSILL AND B. G. HYDE, *Acta Cryst.* **B27**, 210 (1971).
22. P. GADÓ AND L. IMRE, *Acta Chim. Acad. Sci. Hung.* **46**, 165 (1965).
23. H. G. BACHMANN, F. R. AHMED, AND W. H. BARNES, *Z. Krist.* **115**, 110 (1961).
24. R. GRUEHN, *J. Less-Common Metals* **11**, 119 (1966).
25. L. KIHLBORG, *Acta Chem. Scand.* **21**, 2495 (1967).
26. S. ANDERSSON, *Acta Chem. Scand.* **18**, 2233, 2339 (1964).
27. H. A. EICK AND L. KIHLBORG, *Acta Chem. Scand.* **20**, 1658 (1966).
28. A. MAGNÉLI, S. ANDERSSON, L. KIHLBORG, S. ÅSBRINK, S. WESTMAN, B. HOLMBERG, AND C. NORDMARK, Final Technical Report DA-91-591-EUC-935, 1959.